Mater. Res. Soc. Symp. Proc. Vol. 955 © 2007 Materials Research Society **0955-I08-04**

Properties of InN grown by High Pressure CVD

Mustafa Alevli[1,*], Goksel Durkaya[1], Ronny Kirste[1,2] Aruna Weesekara[1], A.G.U. Perera[1], William Fenwick[3], Vincent T. Woods[3], Ian T. Ferguson[32], Axel Hoffmann[2], and Nikolaus Dietz[1]
[1] Georgia State University, Department of Physics & Astronomy, Atlanta, GA 30303
[2] Technical University Berlin, Department of Physics, Berlin, FRG
[3] Georgia Institute of Technology, School of ECE, Atlanta, GA 30332

ABSTRACT

Indium nitride (InN) and indium-rich group III-nitride alloys are promising for a variety of advanced optoelectronic device applications. Embedded indium-rich alloys in wide-bandgap group III-nitrides, e.g. GaAlN, are essential for the fabrication of monolithic integrated light emitting diodes that are tunable in the whole visible spectral region, as well as advanced high speed optoelectronics for optical communication operating. The present limitation in the formation of embedded indium-rich group III-nitrides arise from the dissimilar processing windows in growth of GaAlN versus InGaN at traditional low-pressure growth techniques. In the work, a novel *"high-pressure chemical vapor deposition"* (HPCVD) system is employed, which enables the control of the partial pressures of the InN constituents at processing conditions similar to GaN. The structural analysis of InN layer deposited by HPCVD revealed high-quality, single phase InN(0002) layers with full width half maximum (FWHM) around 385 arcsec for layers grown on GaN/sapphire templates. Raman, transmission and IR reflection spectroscopy are used to study the structural and optical properties of InN thin films grown on sapphire (0001) and GaN/sapphire substrates. The modeling of the transmission spectra by a Lorentzian oscillator model indicates an absorption edge between 1.5 eV and 1.1 eV, with two absorption centers at 1.2 eV and 0.8 eV. The strength of these two absorption centers correlates with the employed precursor ratio, the origin of which is not completely understood at present. The free carrier concentrations in the layers are presently in the mid 10^{19} to low 10^{20} cm^{-3}, as determined by IR-reflectance and Raman A_1 analysis. A reduction of external impurities will be required to further improve the InN material quality. The processing window used for InN growth by HPCVD enables for the first time the fabrication of embedded indium-rich group III-nitride heterostructures.

INTRODUCTION

Group III-nitride compound semiconductors alloyed from their binaries AlN, GaN, and InN enable unique device structures ranging from IR to the deep UV wavelength range. While the materials quality for GaN-AlN compounds and alloys are already at a device fabrication level, the physical properties of InN and indium-rich alloys are still strongly process dependent and far from being integrated in GaAlN wide bandgap heterostructures[1-2]. At present, two of the most severe problems are related to the surface termination of indium-rich InGaN layers and secondly the large thermal decomposition pressures in InN which limits the growth temperatures for low-pressure deposition techniques at and below 500°C, which is at least 200°C lower compared to GaN growth. Even though recent results of InN layers grown by off-equilibrium plasma assisted MBE demonstrated that high-quality InN layers can be achieved with low-pressure deposition techniques, the integration of such layers into wide bandgap group III-

nitrides heterostructures is an unsolved problem. Thermodynamic estimates suggest that the surface for highly volatile compounds such as InN and related alloys can be stabilized at much higher temperatures if stabilized at high pressures of the volatile gas species. This principle evoked the development of a unique *high-pressure CVD* system[3,6-17] at Georgia State University (GSU). The aim of our present research focuses on the growth of InN in an intermediate pressure regime, around 15 bar, at which laminar flow conditions can be maintained[7]. The HPCVD system utilizes reactor pressures up to 100 bar counteract the decomposition of constituents and thereby stabilizes the surface at optimum growth temperatures. Real-time optical diagnostic techniques are utilized to monitor gas phase kinetics as well as growth surface chemistry processes in order to gain insights in the growth kinetics. We demonstrated that this approach successfully suppresses the InN decomposition at growth temperatures between 850°C - 900°C[8,9], which is a major step toward merging the processing windows of indium-rich group III-nitride layers with GaN and AlN processing conditions. The higher growth temperature also improves the crystalline quality of the InN layers and allows the stabilization of indium-rich alloys, which would phase-segregate under low-pressure growth conditions.

EXPERIMENT

The InN layers analyzed in this contribution are grown by HPCVD, utilizing a high-pressure flow channel reactor that is embedded in to an outer reactor which confines a reactor pressure from 1 bar up to 100 bar with integrated real time optical monitoring in order to study and optimize the InN nucleation and growth. The details of the HPCVD system have been described elsewhere[4,10,11]. A special designed pulsed injection scheme utilizing pulse width between the precursors trimethylindium (TMI) and Ammonia (NH_3) with a cycle sequence time 6 sec. is used to minimize the gas phase reactions and the tailoring surface chemistry are being monitored with real time UV absorption spectroscopy and principle angle reflectance spectroscopy. The pulsed precursors are embedded and temporarily controlled in a high-pressure carrier stream, consisting of ultra-pure nitrogen. Not only the total gas flow through the reactor but also the reactor pressure are kept constant during the growth of InN. For the growth results presented here the reactor pressure was 15 bar, gas flow was 12 slm. The precursor flow ratio are evaluated for molar ratio ammonia to TMI from 600 to 1500 in the growth temperature of 1080 to 1150 °K. The temperature setting refers to the correlation of the analyzed black body radiation as a function of the power setting of the substrate heater and is not corrected for the change in surface emissivity during the growth.

RESULTS AND DISCUSSION

Figure 1. shows the structural quality of epitaxially grown InN films, which have been characterized by Θ-2Θ X-ray diffraction scans and Raman Spectroscopy. The samples grown on Sapphire and GaN/Sapphire show very strong XRD peaks centered at $2\Theta=31.3°$ which is corresponding to diffraction of the hexagonal phase InN(0002) plane. However some samples show a small XRD (101) peak at the upper angle side $2\Theta\sim33$ indicate the presence of a second phase. The best full width at half maximum (FWHM) of InN(0002) peaks are 385 and 492 arc sec for the single phase InN deposited on the GaN/Sapphire and Sapphire substrates, respectively. The analysis of XRD data on ref lection planes for the InN films provided the

lattice constants c= 5.40 Å, a= 3.57 Å. These values are in close proximity with the reported values [12].

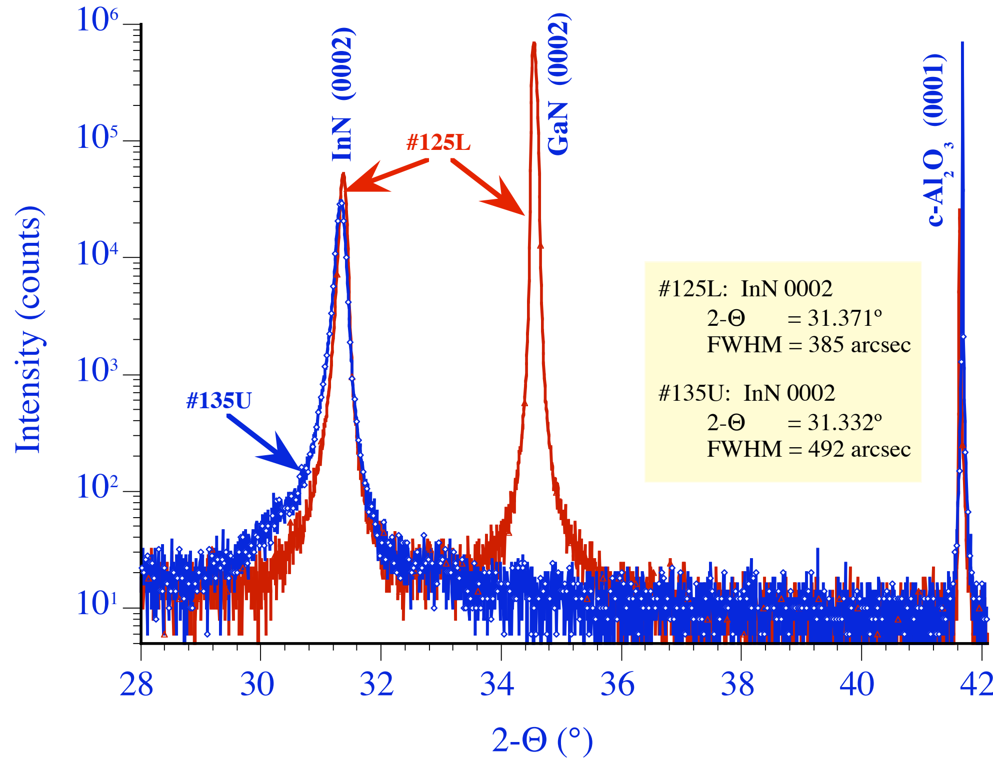

Figure 1:

XRD spectra for InN layers grown on sapphire substrate (135U) and virtual GaN/Sapphire substrate (125L)

Raman spectra of the samples are obtained in backscattering geometry for excitation energy of 2.33 eV and underlying A_1 phonon modes are simulated for a wave-vector non-conserving mechanism by using Lindhard-Mermin approach as considering deformation potential associated with allowed electro-optic (DP+EO) scattering mechanism. The general form of the dielectric function used for numerical calculations is given by[13,14]

$$\varepsilon(q,\omega) = \varepsilon_\infty (1 + \frac{\omega_L^2 - \omega_T^2}{\omega_T^2 - \omega^2 - i\omega\gamma_p} + \frac{(1 + i\Gamma_e/\omega)\chi_e^0(q,\omega + i\Gamma_e)}{1 + (i\Gamma_e/\omega)\{\chi_e^0(q,\omega + i\Gamma_e)/\chi_e^0(q,0)\}}) \quad (1)$$

where Γ_e corresponds to inverse lifetime time of the carriers and $\chi_e^0(q,\omega)$ is the temperature dependent Lindhard susceptibility[16] which takes Fermi distribution and Fermi energy of an electron gas into account at a specific temperature. The intensity and line-shape of the A_1(LO) phonon mode are simulated by considering spectral line shape function weighted by Yukawa-type impurity potential. The best-fit approximations of experimental data for two different samples are presented in Figure 2 with the corresponding Lorentzian fitting parameters given in the inset tables. The line shape simulated with the DP-EO mechanism is showing a small asymmetry on the low asymmetry on the low frequency side with respected to the other mechanism that we have investigated and given in literature. The analysis depicted in Fig. 2 illustrates that best agreement is found between experimental and calculated spectra by considering $q_{\max} = 10q_{TF}$.

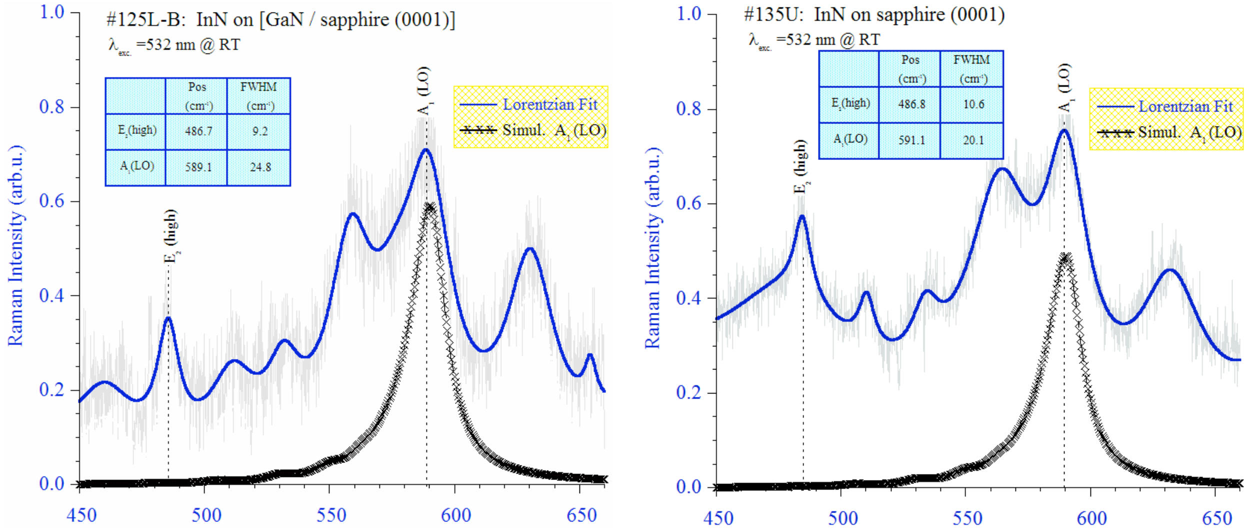

Figure 2. Experimental Raman spectra and simulated A_1(LO) phonon mode of samples (a) 111U-A and (b) 135U-C

Figure 3 depicts the Infrared reflectance Spectrum for sample 135U and the analysis of optical properties in the IR region. The dielectric functions of the InN layers are modeled using Eq. (1) assuming two contributions, one of a Lorentz oscillator for phonons and the second one is the classical Drude model for the plasma response of the electron gas and its damping. The damped dielectric function is given by

$$\varepsilon(\omega) = \varepsilon_\infty + \sum_i \frac{s_i\left(\omega_{TO}^2 - \omega_{LO}^2\right)}{\omega_{TO}^2 - \omega^2 - i\cdot\omega\cdot\Gamma_i} - \frac{\varepsilon_\infty \cdot \omega_p^2}{\omega^2 + i\cdot\omega\cdot\gamma_p}, \tag{2}$$

where γ_p is the electron damping due to the scattering from randomly distributed stationary impurities, ω_p is the plasmon frequency, $\omega_{TO,}$ S_i and Γ_i are the frequency, oscillator strength, and damping parameter of the *i*-th oscillator, ε_∞ is the dielectric response in the high-energy limit for the film. The frequencies ω_{TO} and ω_{LO} of the LO and TO phonon modes were kept constant at 479 and 593 cm^{-1}, respectively. The electron effective mass of InN was set constant to $0.09m_0$[15], neglecting the functional dependency with the free carrier concentration. The change of the electron effective mass as a function of the free carrier concentration is not taken into account. The detail of the calculation method has been published elsewhere[9].

Transmittance is fitted by applying the Model Dielectric Function (MDF) Model[18]. A modified MDF model is used with two added oscillator at ≈0.8 and ≈ 1.2 eV, providing an excellent fit of the experimental transmission spectra

$$\varepsilon_{InN}^{'}(\omega) = \varepsilon_{InN} + \sum_{n=1}^{2} \frac{s_{ab}}{\left[E_{ab}^{\;2} - (\hbar\cdot\omega)^2\right] - i\cdot\hbar\cdot\omega\cdot\Gamma_{ab}}, \tag{3}$$

where S_{ab} is the strength, E_{ab} is the energetic position and Γ_{ab} is the damping of the Lorentzian. The optical constants, structural properties, sample thickness, carrier concentration determined by fitting transmission, reflection and Raman spectrum. All of those values presented in Table I.

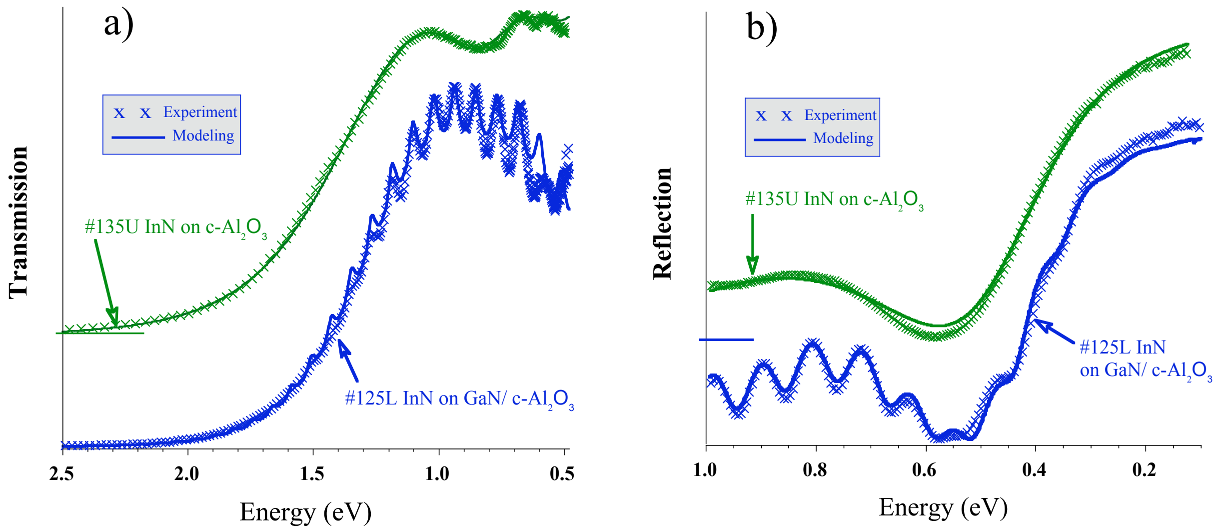

Figure 3. a) Transmission spectra and b) IR reflectance spectra and their best fits for InN layers deposited on sapphire and GaN/sapphire substrates.

Table I. Model fitting parameters for IR reflection, transmission, and Raman spectroscopy

Sample	#125 L			#135U		
	IR	Trans	Raman	IR	Trans	Raman
d_{InN} (nm)	365	305	-	228	210	-
ε_∞	7.5	-	8.3	7.1	-	8.6
ω_p (cm^{-1})	3494	-	3441	3720	-	3907
n (cm^{-3}) 10^{20}	0.9	-	1.0	1.0	-	1.04
μ (cm^2/ Vs)	266	-	-	327	-	-
E_0 (eV)	-	1.42	-	-	1.37	-
γ (cm^{-1})	390	-	368	317	-	431

CONCLUSION

InN films of high crystalline quality have been grown by HPCVD. The free carrier concentration are found to be in the upper 10^{19} to lower 10^{20} cm^{-3} with the corresponding optical absorption edge in between 1.4 to 1.6 eV. A reduction of remaining residual impurities will be required to further reduce the free carrier concentration in the layers. The modeling of the IR-reflectance data suggest the present of two distinct InN layers: one with electron concentrations below $5x10^{17}$ cm^{-3}, which is followed by a second layer in the upper 10^{19} cm^{-3} closer to the surface. Further studies are needed to identify the role of oxygen impurities and the position of associated defect energies with respect to the InN band structure. All our experimental data show that shift in the absorption edge is not direct related to the free carrier concentration, ruling out a postulated Moss–Burstein effect as leading cause for the observed bandgap shift. The roles of extrinsic impurities as well as stoichiometry deviation and the associated point defect chemistry will need further studies in order to gain a better insight and control in the encountered deviations.

REFERENCES

[1] K. Scott, A. Butcher, M. Wintrebert-Fouquet, P. P.-T. Chen, K. E. Prince, H. Timmers, S. K. Shrestha, T. V. Shubina, S. V. Ivanov, R. Wuhrer, M. R. Phillips, and B. Monemar, Phys. Stat. Sol. (c) **2**, pp. 2263-2266 (2005).

[2] Dimiter Alexandrov, K. Scott A. Butcher and Trevor L. Tansley, J. Cryst. Growth **288** pp. 261-267 (2006).

[3] N. Dietz, S. McCall, K.J. Bachmann, Proc. Microgravity Conf. 2000, NASA/CP-2001-210827, pp. 176 -181 (2001).

[4] N. Dietz, V. Woods, S. McCall and K.J. Bachmann, Proc. Microgravity Conf. 2002, NASA/CP-2003-212339, pp. 169 -181 (2003).

[5] V. Woods and N. Dietz, Mater. Sci. & Eng. B **127**(2-3) pp 239-250 (2006).

[6] N. Dietz, book chapter 6 in “III-Nitrides Semiconductor Materials”, ed. Z.C. Feng, Imperial College Press, ISBN 1-86094-636-4, pp. 203-235 (2006).

[7] V. Woods, H. Born, M. Strassburg and N. Dietz, J. Vac. Sci. Technol. A **22** (4), pp. 1596 - 1599 (2004).

[8] N. Dietz, M. Alevli, V. Woods, M. Strassburg, H. Kang, and I. T. Ferguson, Phys. stat. sol. (b) **242**(15) pp. 2985-2994 (2005).

[9] M. Alevli, G. Durkaya, W. Fenwick, A. Weerasekara, V. Woods, I. Ferguson, A.G.U. Perera and N. Dietz, Appl. Phys. Lett. **89**, pp. 112119 (2006).

[10] B. H. Cardelino, C. E. Moore, C. A. Cardelino, and N. Dietz, Proc. SPIE Vol. **5912**, ISBN 0-8194-5917-8, pp. 86 - 99 (2005).

[11] N. Dietz, M. Alevli, H. Kang, M. Straßburg, V. Woods, I. T. Ferguson, C. E. Moore and B. H. Cardelino, Proc. SPIE Vol. **5912**, ISBN 0-8194-5917-8, pp. 78-85 (2005).

[12] T.L. Tansley and C.P. Foley, J. Appl. Phys. **59**(9) pp. 3241-4 (1986).

[13] F. Demangeot, C. Pinquier, J. Frandon, M. Gaio, O. Briot, B. Maleyre, S. Ruffenach, and B. Gil, Phys. Rev. B **71**, pp.104305-11 (2005).

[14] U. Fano, Phys. Rev. **124**(6) pp.1866 - 1878 (1961).

[15] T. Inushima, M. Higashiwaki, and T. Matsui, Phys. Rev. B **68**, 235204 (2003).

[16] David Pines, “Elementary Excitations In Solids,” Perseus Books, ISBN: 0805379134 (1963)

[17] M. Alevli, G. Durkaya, V. Woods, U. Habeck, H. Kang, J. Senawiratne, M. Strassburg, I. T. Ferguson, A. Hoffmann, and N. Dietz, Mat. Res. Soc. Symp. Proc. **892**, ISBN: 1-55899-846-2, FF6.2, pp.1-6 (2006).

[18] T. Kawashima, H. Yoshikawa, S. Adachi, S. Fuke, and K. Ohtsuka, J. Appl. Phys. 82(7) pp.3528-3535 (1997).